IS-PORTO 2023 PROCEEDINGS

Proceedings of the 8th International Symposium on DEFORMATION CHARACTERISTICS OF GEOMATERIALS Porto, 3rd - 6th September 2023

Use of computer vision to analyze cyclic loads on the Guamo sand

Diego Gil[1], *Cristhian* Mendoza[1#], and *Luis* Vásquez-Varela[1]

[1]*Universidad Nacional de Colombia, Department of Civil Engineering, Cr 27 # 64-60, Colombia*
[#]*Corresponding author: cmendozab@unal.edu.co*

ABSTRACT

Some effects have been evidenced during several earthquakes around the world. For example, the liquefaction phenomenon, and structural collapse, among others. However, granular soil behaviour during this event has not been completely understood; this is proved by the number of investigations in physical models, constitutive models, and laboratory testing proposals about this topic. A question appears at this point: when do the effects take place? To cope with this issue, it is proposed to create an experimental model composed of a Single Degree of Freedom Oscillator (SDOFO) designed to try to assess the liquefaction. Likewise, the device could transmit cyclic loadings to the soil. This SDOFO was an electromechanical oscillator servo-controlled appropriated to manage the frequency of excitation and amplitude of the oscillatory movement. The measurement methodology was based on computer vision using Open CV by Python, which allowed measuring displacements and times of the SDOFO instead of using LVDT sensors located directly at the actuator; thus, computer vision permitted a "free movement" of the actuator similar to the actual behaviour of buildings in seismic events. The samples required for this study were the Guamo sand collected in a natural deposit in Colombia (South America) and the Ottawa sand to compare results. A simple criterion was used to try to determine the possible liquefaction onset. It was defined based on the evolution of displacements relying on the number of cyclical loads. According to the results, it was able to define that the relationship between the excitation frequency, the amplitude of the oscillatory movement, and the number of cycles required to reach the possible liquefaction state was inverse.

Keywords: Computer vision; experimental model; liquefaction.

1. Introduction

Seismic events are natural hazards responsible for significant loss of life and structural damage (Elnashai & Di Sarno 2008) and generate risk scenarios for populations (Bevere et al. 2019).

Liquefaction is a natural process related to saturated cohesionless soils undergoing rapid loading under undrained conditions, where the tendency for densification causes pore pressures to increase and effective stress to decrease (Kramer 1996). There are several methodologies and criteria for assessing flow liquefaction and cyclic mobility: geological (Youd & Perkins 1978), historical (Verdugo 2015), compositional (Bray & Sancio 2006), double axial strain triaxial (Ishihara 1993), pore water pressure ratio r_u (Wu et al. 2004), and energy-based criteria (Azeiteiro et al. 2017), among others.

The dynamic soil behaviour and the liquefaction phenomenon have been studied employing SDOF systems with rocking vibration mode (Anastosopoulos 2011; Anastasopoulos et al. 2012; Gazetas 2015; Martakis et al. 2017; Taeseri et al. 2018; Jafarian et al. 2021). This paper tries to understand the liquefaction process triggered by dynamic loads by the evolution of displacements.

This research employs an experimental model of a shallow square foundation, which can induce cyclical loads on a saturated granular soil sample, to try to evaluate its behaviour at liquefaction based on excitation frequency and amplitude of the vertical displacement in the edge of the square footing. The research presents a series of cyclic excitation tests with variable excitation frequency and amplitude of the oscillatory movement. Servo-controlled harmonic loads were controlled and applied through an Arduino Uno plate, and computer vision routines, coded in the Python programming language, were used to record and process data. The paper describes the data recording, processing, and analysis related to liquefaction phenomena.

This study searches to evaluate the Guamo and the Ottawa sands to compare their number of cycles to reach a possible liquefaction onset. This last was defined by applying a simple criterion relying on the vertical displacement progression on the edge of the square footing. Results showed that the excitation frequency and the amplitude of the oscillatory movement inversely influence the liquefaction occurrence. Also, the effective grain size, D_{10}, inversely influences the number of cycles at liquefaction.

2. Experimental setup

2.1. Previous Experimental SDOF models

Earthquake engineering has used SDOF models to simulate the behaviour of complex structural systems (Baltzopoulos et al. 2018). Several researchers employed SDOF models to study soil behaviour on cohesionless

and cohesive soils. Al-Wakel et al. (2014) performed a systematic experiment to investigate the dynamic response of a machine foundation on saturated soil under a vertical vibration mode, however, in the experimental set-up introduced in this paper, the experimental analysis was accomplished under a rocking mode of vibration. This vibration mode was used by several researchers as mentioned below. Martakis et al. (2017) investigated the influence of soil properties and structural parameters on the Soil Structure Interaction (SSI) effect with an SDOF model in multiple centrifuge tests. The dynamic experiments were used to verify analytical models for soil damping and stiffness prediction. Taeseri et al. (2018) studied small-strain foundation response based on centrifuge model tests. An SDOF model with a rocking mode of vibration was used to study the seismic performance of shallow and embedded foundations on flat and sloping soil and to verify the analytical formulations related to the shear modulus distribution with depth in sand. Gavras et al. (2020) compile the results of five centrifuge tests and three shaking table tests from the United States, Greece, and Japan to assess several SDOF physical models under a rocking vibration mode. Jafarian et al. (2021) compared the soil layer response in containers with fixed-end and flexible boundary conditions on the boundaries. They used a saturated loose sand sample and an SDOF superstructure on a shallow foundation model and assessed the liquefaction by computing the pore water ratio, r_u, at several depths from the surface sample employing a pore water transducer. Similarly to the last four research shown above, herein, a study of rocking mode vibration in shallow foundations is presented. This research is remarkable because the uplift and sinking of the shallow foundation can reduce the force and ductility demands transmitted to the superstructure.

2.2. Testing device

The authors developed the experimental model to try to achieve a better understanding of the number of cycles required to reach a possible liquefaction onset on a saturated granular soil according to the excitation frequency and the amplitude of the vertical displacement in the edge of the square footing, subject to the granulometric distribution and particle shape, among other soil characteristics.

Fig. 1 shows the experimental setup required to test the sand samples. The device comprises an acrylic box to store the sample, an acrylic box used to store water, a hose to link both boxes, valves to regular water entry, levels, clamps, laboratory stand supports, a static target of 20 by 20 mm, control plate, camera, PC with Arduino IDE and any IDE able to run Python codes.

Fig. 2 shows the SDOFO composed of a dynamic target of 20 by 20 mm, bearings, rigid connections, column, torque mass, and square footing.

The square foundation and the column steam were built using steel. The bottom of the footing was roughened using sandpaper to provide friction; thus, there was no sliding under loading.

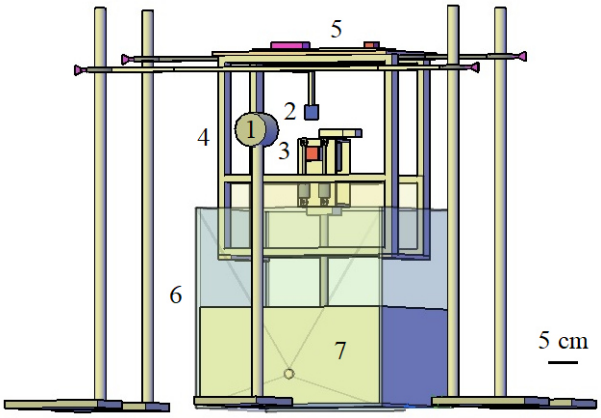

Figure 1. Experimental setup: (1) camera, (2) static target, (3) dynamic target, (4) guides, (5) electronic compounds, (6) sample box, and (7) sand sample.

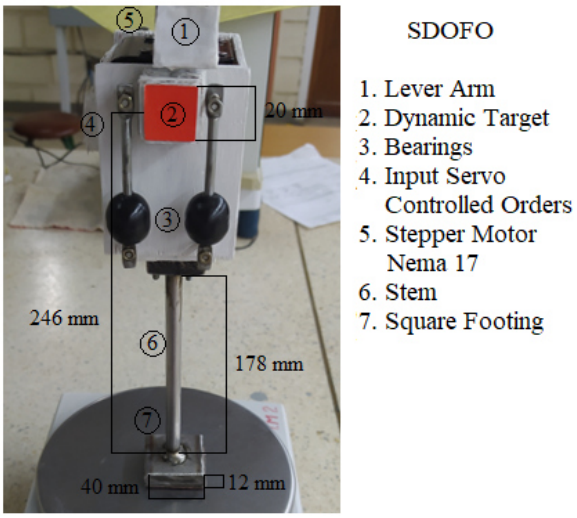

Figure 2. Photograph of the SDOFO.

Table 1 summarizes the dimensions of the SDOFO components.

Table 1. Dimensions of the SDOFO components.

Parameter	Value	Units
Depth of embedment	40	mm
Width of the square footing	40	mm
Foundation half-width	20	mm
Square footing thickness	12	mm
Height of the column	178	mm
Bending stiffness of the column	430	MPa*m
SDOFO column natural frequency	3669	Hz
Effective height of the equivalent SDOF model	246	mm
Actuator total mass	808.47	g
The critical angle for a rigid structure on a rigid base	0.081122	rad

A rigid block can represent a shallow foundation in a soil medium with six degrees of freedom. However, the features of the experimental model presented here require just a single degree of freedom; for this purpose, guides were located to constrain three of the six degrees of

freedom. Still, the rocking motion was unique because the sandpaper restricted the lateral motion, and the vertical motion was considered constant because the settlement of the SDOFO on the sand was assumed instantaneous.

The authors prepared the soil samples by the dry air pluviation method following the procedure used by Molina-Gómez & Viana (2021). Deaereated water was obtained by boiling tap water and storing it in a sealed container to saturate the samples (Ruelke 2010). The water surface reached 20 mm above the sample surface, and 24 hours were required to achieve a saturation close to 1.0, according to Eq. (1):

$$S = \frac{\omega}{\omega_{max}} \quad (1)$$

where ω is the water content, and ω_{max} is the maximum water content.

If a sample were not fully saturated, the liquefaction resistance would be higher than in a saturated sample because the air in the voids will compress before the water during cyclic loading. Consequently, the sand liquifies after the air has dissolved into the solution from cyclic loading, increasing liquefaction resistance.

The vertical displacement in the edge of the square footing was computed with Eq. (2) by converting the position of the dynamic target centroid related to the static target centroid for every recorded displacement, as shown in Fig. 3:

$$\delta = \Delta * \{(B/2)/H\} \quad (2)$$

Where δ is the vertical displacement in one of the edges of the square footing, Δ is the horizontal movement of the dynamic target concerning the static target, B is the width of the square footing, and H is the effective height of the equivalent SDOF model.

Two Python algorithms interpret the information recorded by the machine vision system. The first algorithm finds a scaling factor suitable to convert pixels into millimeters using the measures of the static target dimensions as a calibration process. The second algorithm reads and stores data about the position of the centroid of the dynamic target and the centroid of the static target in each video frame.

The main parameters and functions employed in this research were:

1. kernel: a kernel matrix in computer vision is a small matrix used to apply effects such as blurring, sharpening, outlining, or embossing. In machine learning is employed to select characteristics from an image (Powell, 2022).
2. cv2.cvtColor: this function let to change the BGR image format to HSV image format, which was suitable to define ranges of color based on its Hue, Saturation, and Value. This is because, HSV color space is the most suitable color space for color-based image segmentation (OpenCV Lessons, 2010).
3. cv2.morphologyEx: Morphology transformations are operations normally performed on binary images based on the image shape, two inputs are required to apply this transformation a) original image, b) kernel. Specifically, the transformation employed was Opening, this operation first applies an erosion and later a dilation. It is useful in removing noise (OpenCV24, 2016).
4. cv2.moments: this function serves to compute the centroid of a binary image; it is used to relate the motion between two consecutive images. The function detects features on an image that remains unchanged when the object undergoes rotation, translation, or any other form of orientation (Python pool, 2021).
5. cv2.convexhull: An object is convex when it is curved outward, in other words, the object does not have interior angles greater than 180 degrees. Convex Hull of a concave object or a group of points is a tight-fitting convex boundary around the points or the shape. Therefore, the convex hull of a convex object is its boundary, however, the convex hull of a concave object is a convex boundary that most tightly encloses it (Ravi, 2018).

Computer vision allows indirect measuring of displacements instead of using LVDT sensors which have a different rigidity than the sample and may affect the test results (Zhao et al. 2020).

The camera used to capture the movement was an HP Pro Webcam with a video resolution of 640 x 480 4:3 at up to 30 frames per second and a power line frequency anti-flicker of 60 Hz.

Optical distortions such as barrel, pincushion, and wavy distortion were insignificant

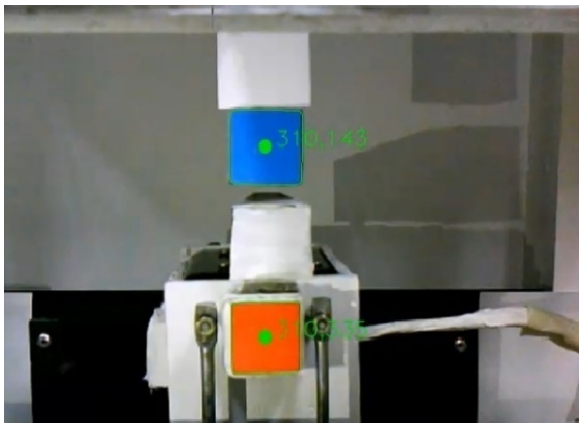

Figure 3. Static and dynamic targets centroids identification by computer vision. The green point depicts the centroid and the numbers on the right side are the x coordinate and the y coordinate in pixels from the left upper corner.

2.3. Soil Characterization

Samples corresponded to two types of sand: (a) Guamo sand from a natural deposit located at geographic coordinates 4°02'00.0" N 74°57'24.0" W in Colombia, and (b) Ottawa sand conforming to ASTM C87, C109, C348, C359, C593, and C778 standards. "Table 2" summarizes some of the properties of these soils.

Several authors studied Guamo sand in Colombia (Núñez 1996; Murcia & Hurtado 2003; Patiño 2006; Lizcano & Jimenez 2015; Ruiz & Bermudez 2015; and Tique 2016). The mineralogy of Guamo sand is composed of pyroclastic fragments and quartz; other components are sedimentary and plutonic fragments, feldspar, and hornblende.

Table 2. Guamo and Ottawa sands characteristics

Properties	Guamo sand	Ottawa sand
Uniformity Coefficient [-]	3.28	1.57
Coefficient of Curvature [-]	0.99	0.96
Mean grain size [mm]	0.60	0.43
Effective grain size	0.25	0.30
Fines Content [%]	0	0
Specific Gravity [-]	2.55	2.67*
Permeability coefficient [cm/s]	0.0026	0.0409
Maximum void ratio [-]	0.59	0.72
Minimum void ratio [-]	0.36	0.48
Void ratio [-]	0.556	0.683
Shear wave velocity [m/s]	-	175*
Soil natural frequency [Hz]	-	292
Effective soil friction angle [°]	35.35	30.41
Effective soil cohesion [kPa]	0	0
Soil classification	A-1-b	A-3
Soil classification	SP	SP

*Data were taken from Cunning et al., (1995).

Ottawa sand is clean quartz sand. Fig. 4 shows the granulometric curves, between 4.75 mm and 75 µm, for the two types of sand without fines.

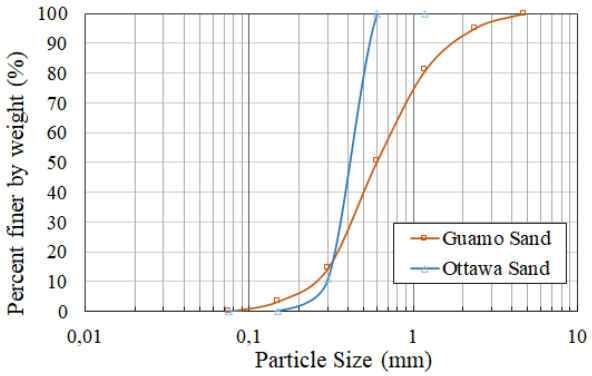

Figure 4. Grain size for Guamo and Ottawa sands.

Cho et al. (2006) proposed that increasing particle regularity (sphericity or roundness) leads to a decrease in extreme void ratios e_{max} and e_{min}, which are required to calculate relative density. Patiño (2006) reported that liquefaction susceptibility for soil mixtures decreases with increasing relative density. Therefore, the particle shape influences the liquefaction process.

Cho et al. (2006) stated that the particle shape is another significant soil index property and proposed a methodology to determine sphericity and roundness. That methodology is used in this work, so it was possible to observe the variability of sphericity and roundness concerning grain size (Fig. 5). The results show a direct proportion between roundness and grain size; however, sphericity does not present a trend.

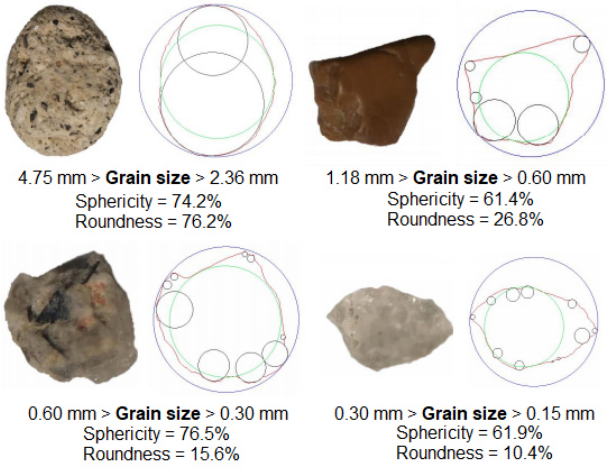

Figure 5. Guamo sand roundness and sphericity.

3. Results and Discussion

This section analyzes the behaviour of the amplitude of the vertical displacement in the edge of the square footing, the excitation frequency applied by the electromechanical oscillator, and their relationship with the number of cycles required to reach the possible liquefaction considering a criterion based on displacement evolution.

3.1. Vertical displacement amplitude

One of the general liquefaction criteria for laboratory and experimental tests is to report the sand behaviour in terms of a fatigue model (Jefferies & Been 2006). Liquefaction is usually determined using the 5% double amplitude (DA) axial strain criteria in Cyclic Triaxial (Ishihara 1993). Also, a common way to determine the liquefaction process is with the ratio of pore water pressure r_u. Liquefaction occurs if r_u is equal to one since Δpw equals σ_{v0}, since $\sigma' = \sigma_{v0} - \Delta pw = 0$. However, pore pressure-based liquefaction has some drawbacks: (a) $r_u = 1.0$ is not always reached, even at large strains, but liquefaction happens, and (b) Δpw measuring in laboratory experimentation is difficult when the loading rate is high relative to the rate at which pore pressures equalize across the specimen (Wu et al. 2004). Wu et al. (2004) also conclude that "in most field liquefaction cases, investigators instead rely on manifestations of liquefaction observable at the ground surface."

The authors did not employ pore water pressure sensors. Therefore, a criterion based on displacement evolution was used to recreate the actual dynamical behaviour of a slender structure as well as possible.

Fig. 6 shows a linear trend in the first part of the maximum vertical displacement on the edge of the footing (MVDEFC) per cycle.

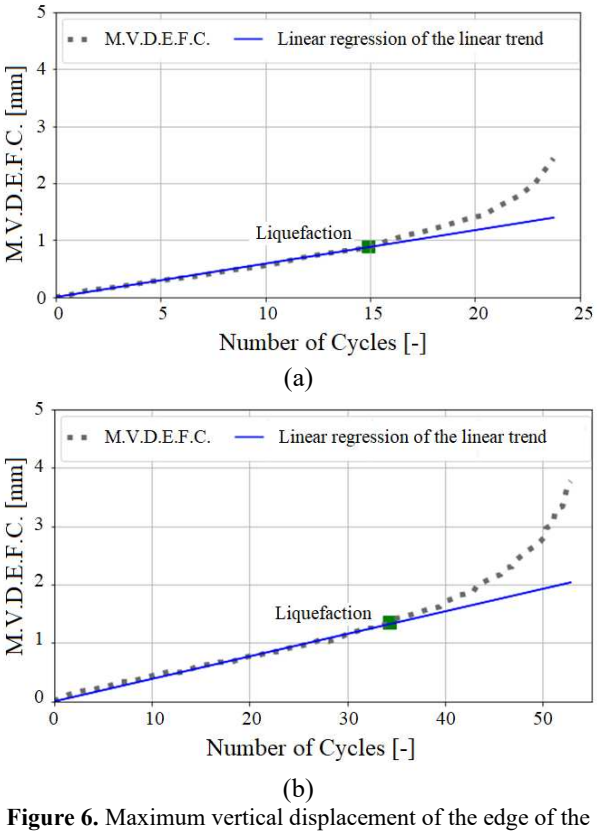

Figure 6. Maximum vertical displacement of the edge of the footing per cycle (MVDEFC) versus the number of cycles. (a) Ottawa sand at 5.28 Hz - 0.13 mm (amplitude of the vertical displacement in the edge of the square footing), number of cycles at liquefaction = 15, R^2 for linear trend = 0.926; (b) Guamo sand at 5.32 Hz - 0.13 mm (amplitude of the vertical displacement in the edge of the square footing), number of cycles at liquefaction = 35, R^2 for linear trend = 0.915.

The left part of the graph shows a linear trend between the maximum vertical displacement of the footing and the number of cycles, but later, these curves separate from each other. This deflection shows an accelerated increment of the vertical displacements in the edge of the footing as long as the number of load cycles, which could suggest a possible liquefaction onset. This separation corresponds to a coefficient of determination, R^2, of the last portion of the overlapped linear trend smaller than 0.95 but greater than 0.90. The possible liquefaction onset was assumed when the maximum vertical displacement on the edge of the footing is equal to or greater than 2.5 % of the linear trend for the same loading cycle after the separate state. The value of 2.5% was used as a way to try to have a relation with the Doble Amplitude criterion. Eq. (3) presents the mathematical definition.

$$\frac{\delta - \delta_{linear}}{\delta_{linear}} \geq 2.5\% \qquad (3)$$

Where δ is the maximum vertical displacement on the edge of the footing per cycle, and δ_{linear} is the linear trend of the first part of the maximum vertical displacement on the edge of the footing.

3.2. Excitation frequency

Fig. 7 shows the relationship between the excitation frequency, the vertical displacement amplitude on the edge of the footing, and the number of cycles at liquefaction for the Ottawa and Guamo sands.

Test frequencies ranged from 2.5 Hz to 6.5 Hz; amplitude ranged from 0.02 mm to 0.25 mm for the vertical displacement on the edge of the footing. It was possible to observe that both excitation frequency and amplitude of the vertical displacement on the edge of the footing were inverse to the number of cycles at possible liquefaction onset.

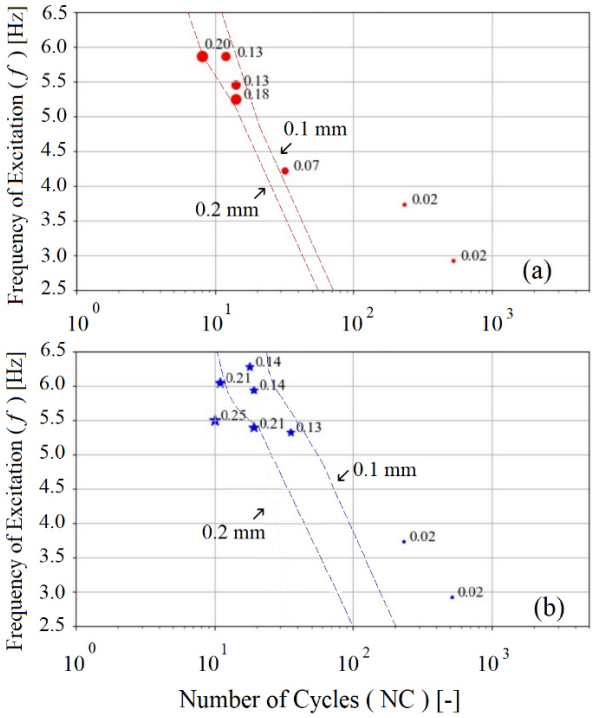

Figure 7. The number of loading cycles (NC) at liquefaction according to the frequency and amplitude of movement on the edge of the footing in oscillatory movement. The annotations in the markers refer to the amplitude on the edge of the footing. The sizes of the markers were proportional to the value of the amplitude on the edge of the footing; (a) Ottawa sand, (b) Guamo sand.

Fig. 8 shows the relationship between the number of loading cycles at possible liquefaction onset (NC), the effective grain size (D_{10}) for frequencies between 2.5 Hz and 6.5 Hz, and a range of vertical displacement amplitudes between 0.1 mm and 0.2 mm. Note that D_{10} influenced the number of cycles at liquefaction, and their relationship was mainly inverse because D_{10} regulates the flow of water through soils and can control their mechanical behaviour since the coarser fractions may not be ineffective in contact with each other; that is, they float in a matrix of finer particles (Budhu 2015).

This figure introduced another result performed on Tumaco sand from Colombia (South America) with a D_{10} equal to 0.15 mm, to depict in a better way the D_{10} and liquefaction onset relationship.

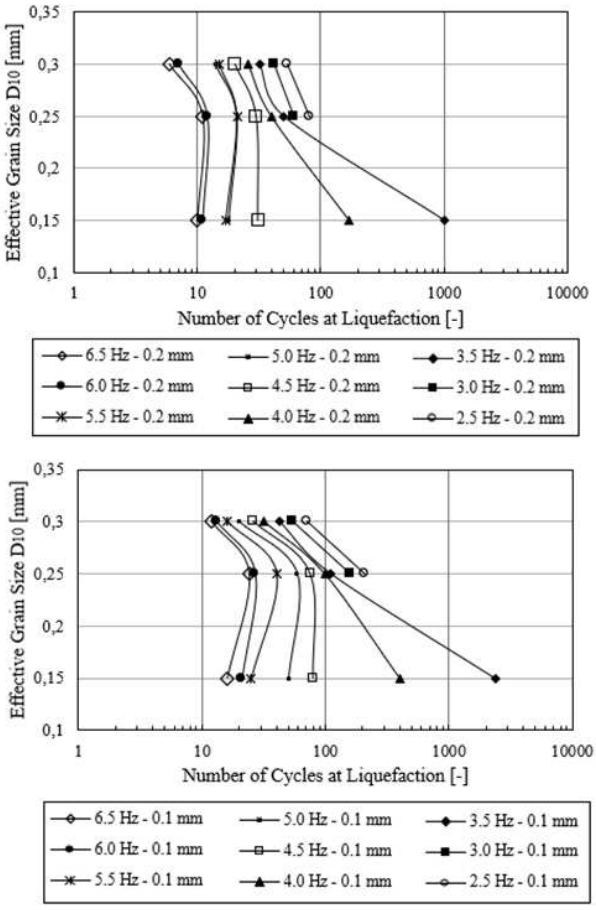

Figure 8. The number of cycles at liquefaction (NCL) versus effective grain size D_{10}. It is possible to observe the influence of D_{10} on the behaviour of the sand samples subjected to specific excitation frequencies and vertical displacement amplitudes on the edge of the footing.

Table 3 summarizes the results obtained for all tests on both types of sand.

Table 3. Results from Ottawa and Guamno sands test

Sand	Frequency f [Hz]	Amplitude δ [mm]	Number of Cycles [-]	R^2
Ottawa	2.92	0.02	557	0.943
Ottawa	3.73	0.02	255	0.908
Ottawa	4.22	0.07	36	0.945
Ottawa	5.25	0.18	17	0.935
Ottawa	5.28	0.13	15	0.926
Ottawa	5.45	0.13	17	0.938
Ottawa	5.86	0.13	14	0.914
Ottawa	5.86	0.2	11	0.944
Guamo	2.93	0.02	564	0.945
Guamo	3.73	0.02	279	0.906
Guamo	5.32	0.13	34	0.915
Guamo	5.39	0.21	20	0.935
Guamo	5.5	0.25	9	0.929
Guamo	5.94	0.14	19	0.947
Guamo	6.05	0.21	12	0.93

4. Conclusions

The vertical displacement amplitude on the edge of the square footing and the excitation frequency influence the number of cycles at possible liquefaction onset. Both, the relationship between the excitation frequency, the vertical displacement amplitude on the edge of the footing, and the number of cycles at possible liquefaction onset were inverse.

Computer vision allows satisfactory indirect measurements of physical parameters in experimental models, laboratory, and experimental field tests.

Acknowledgments

The authors are grateful for the financial support provided by Universidad Nacional de Colombia Sede Manizales throught the project "Modelo físico de licuación en suelos granulares", "Convocatoria para el fortalecimiento de la investigación, creación e innovación articulado con la formación en la Universidad Nacional de Colombia 2020-2021". Also, the authors are grateful to the "Julio Robledo Isaza" Laboratory of Materials at Universidad Nacional de Colombia Sede Manizales for their support, especially to Prof. José O. Jaramillo, Mr. D. Herrera, and Mr. O. Villegas.

References

Al-Wakel, S.F.A; Fattah, M.Y; Karim, H.H; Chan, A.H.C. 2014. Experimental and Numerical Modeling of Machine Foundations on a Saturated Soil. Numerical Methods in Geotechnical Engineering – Proceedings of the 8th European Conference on Numerical Methods in Geotechnical Engineering, NUMGE 2014. The Netherlands.

Anastasopoulos, I., Kourkoulis, R., Gelagoti, F., & Papadopoulos Efthymios. 2012. Rocking response of SDOF system on shallow improved sand: An experimental study. Soil Dynamics and Earthquake Engineering. Vol. 40, pp. 15 – 33. 41.

Anastasopoulos, I., Gelagoti, F.; Kourkoulis, R.; Gazetas, G.; MASCE. 2011. Simplified Constitutive Model for Simulation of Cyclic Response of Shallow Foundations: Validation against Laboratory Tests. J. Geotech. Geoenviron. Eng. ASCE, 37(12), pp. 1154-1168.

Ashmawy, A.K., Sukumaran, B., Hoang, V.V. 2003. Evaluating the Influence of Particle Shape on Liquefaction Behavior Using Discrete Elements Modeling.

Azeiteiro, R.J.N., Cohelo, P.A.L.F., Taborda, D.M.G. & Grazina, J.C.D. 2016. Energy-based evaluation of liquefaction potential under non-uniform cyclic loading. Soil Dynamics and Earthquake Engineering. Vol 92, pp. 650 – 665.

Baltzopoulos, G., Baraschino, R., Iervolino, I., & Vamvatsikos, D. 2018. Dynamic analysis of single-degree-of-freedom systems (DYANAS): A graphical user interface for OpenSees. Engineering Structures, 395 - 408.

Bevere L, Ewald M, Wunderlich S. 2019. A decade of major earthquakes: lessons for business. Zurich, Switzerland: Swiss Re Institute.

Bray, J.D. & Sancio, R.B. 2006. Assessment of the Liquefaction Susceptibility of Fine-Grained Soils. Journal of Geotechnical and Geoenvironmental Engineering. Vol 132, No 9, pp. 1165 – 1177.

Budhu, M. 2015. Soil Mechanics Fundamentals. John Wiley & Sons. The United Kingdom.

Cho, G-Ch., Dodds. J., & Santamarina, J.C. 2006. Particle Shape Effects on Packing Density, Stiffness, and Strength: Natural and Crushed Sands. Journal of Geotechnical and Geoenvironmental Engineering. Vol 132, No 5, pp. 591 – 602.

Elnashai, A.S., Di Sarno, L. 2008. Fundamentals of Earthquake Engineering. John Wiley & Sons. West Sussex. United Kingdom.

Fisher R L. 1974. Pacific-Type Continental Margins. Em C. A. Burk, & C. L. Drake, The Geology of Continental Margins. Berlin, Heidelberg: Springer.

Garnier, J., Gaudin, C., Springman, S. M., Culligan, P. J., Goodings, D., Koning, D., . . . Thorel, L. 2007. Catalogue of scaling laws and similitude questions in geotechnical centrifuge modelling. International Journal of Physical Modelling in Geotechnics, 1-23.

Gavras, A. G.; Kutter, B. L.; Hakhamaneshi, M.; Gajan, S.; Tsatsis, A.; Sharma, K.; Kohno, T.; Deng, L.; Anastosopoulos, I.; Gazetas, G. 2020. Database of rocking shallow foundation performance: Dynamic shaking. Earthq. Spectra, pp. 1-23.

Gazetas, G. 2015. 4th Ishihara lecture: Soil-foundation-structure systems beyond conventional seismic failure thresholds. Soil Dynamics and Earthquake Engineering, 23 - 39. 13.

Iai, S. 1989. Similitude for shaking table tests on soil-structure-fluid model in 1g gravitational field. Soil and Foundations. Vol. 29, No. 1, 105-118.

Ishihara, K. 1993. Liquefaction and flow failure during earthquakes. Géotechnique, 43(3), 351-415.

Jafarian, Y., Esmaeilpour, P., Shojaeemehr, S., Taghavizade, H., Rouhi, S., McCartney, J.S. 2021. Impacts of Fixed-End and Flexible Boundary Conditions on Seismic Response of Shallow Foundations on Saturated Sand in 1-g Shaking Table Tests. Geotechnical Testing Journal. Vol. 44, No. 3 pp. 637 – 664.

Jefferies, M., & Been, K. 2006. Soil liquefaction A critical state approach. London and New York: Taylor & Francis.

Jimenez, O., Lizcano, A. 2015. Liquefaction flow behavior of Guamo sand. Fundamentals to Applications in Geotechnics.

Kramer, S. L. 1996. Geotechnical Earthquake Engineering. Prentice-Hall, Inc. Upper Sanddle River, New Jersey.

Martakis, P., Taeseri, Damoun., Chatzi, Eleni., Laue, Jan. 2017. A centrifuge-based experimental verification of Soil-Structure Interaction effects. Soil Dynamics and Earthquake Engineering, 103, 1 - 14.

Molina-Gómez, F., Viana, A. 2021. Key geomechanical properties of the historically liquefiable TP-Lisbon sand. Soil and Foundations.

Murcia, H. F., & Hurtado, B. O. 2003. Caracterización del depósito de flujo de escombros de Chicoral, volcán Cerro Machín, Colombia. Manizales: Universidad de Caldas.

Nong, Z., Park, S.-S., Jeong, S.-W., & Lee, D.-E. 2020. Effect of Cyclic Loading Frequency on Liquefaction Prediction of Sand. Applied Sciences MDPI, 1-15.

Núñez, A. 1996. Mapa Geológico del Departamento del Tolima. Geología, Recursos Geológicos y Amenazas Geológicas. Escala 1:250.000. Memoria Explicativa. Ibagué.

OpenCV Lessons., (2010). Object Detection Using Color Separation. https://www.opencv-srf.com/2010/09/object-detection-using-color-seperation.html.

Patiño, J. C. 2006. Parámetros Hipoplásticos de la Arena del Guamo-Colombia. Bogotá: Universidad de los Andes.

Pestaña J.M. 2004. Laboratory Study of Liquefaction Triggering Criteria. 13th World Conference on Earthquake Engineering. Paper No. 2580 Vancouver, B.C., Canada.

Powell V., (2022). Image Kernels Explained Visually. Setosa. https://setosa.io/ev/imagekernels/#:~:text=An%20image%20kernel%20is%20a,important%20portions%20of%20an%20image

Ravi K. S., (2018). Convex Hull using OpenCV in Python and C++. https://learnopencv.com/author/krshrimali/

Rees, S. (2020, 09 29). GDS Instruments. Retrieved from GDS Instruments: https://www.gdsinstruments.com/

Ruelke. 2010. Is water more than just H2O? AASHTO re: source (Journal AMRL). http://aashtoresource.org/university/newsletters/newsletters/2016/08/02/is-water-more-than-just-h2o

Ruiz, J. C., & Bermudez, J. F. 2015. Estudio experimental de la línea de inestabilidad bajo condiciones anisotrópicas de carga no drenada monotónica. Bogotá, Colombia: Pontificia Universidad Javeriana.

Srbulov, M. 2008. Geotechnical Earthquake Engineering Simplified Analyses with Case Studies and Examples. UK: Springer Science+Business Media BV.

Stokoe, K. H. 2003. Attachment A-7, Results of Resonant Column/Cyclic Torsional Shear Testing. Austin, Texas: the United States Nuclear Regulatory Commission Site Safety Analysis Report for Exelon Generation Company, L.L.C. Early Site Permit.

Taboada A, Rivera L A, Fuenzalida A, Cisternas A, Philip H, Bijwaard H, Rivera C. 2000. Geodynamics of the northern Andes: subductions and intracontinental deformation (Colombia). Tectonics 19/5, 787 - 813.

Taeseri, D., Laue, J., Martakis, P., Chatzi, E., & Anastasopoulos, I. 2018. Static and dynamic rocking stiffness of shallow footings on sand: centrifuge modeling. International Journal of Physical Modelling in Geotechnics, 18(6), 315 - 339.

Taylor, R. N. 1995. Geotechnical centrifuge technology. New York: Taylor & Francis.

Tique, D.O. 2016. Estudio experimental de la inestabilidad difusa para la arena del Guamo Tolima. Bogotá, Colombia: Pontificia Universidad Javeriana.

Verdugo, R. 2015. Liquefaction Observed During the 2010 Chile Earthquake. Geotechnical, Geological and Earthquake 37. Springer International.Switzeland.

Wu, J.; Kammerer, A.M.; Riemer, M.F.; Seed, RB; Pestana J.M. 2004. Laboratory Study of Liquefaction Triggering Criteria in 13th World Conference on Earthquake Engineering, Vancouver, B.C., Canada.

Youd, T.L. & Perkins, D.M. 1987. Mapping of Liquefaction Severity Index. Journal of Geotechnical Engineering. ASCE, Vol. 113, No 11, pp. 1374 – 1392.

Zhao, H.-h.; Liu, C.; Tang, X.-w.; Wei, H.-w.; Zhu, F. 2020. Study of Visualization measurement system of spatial deformation based on transparent soil and three-dimensional reconstruction technology. Rock and Soil Mechanics, 41(9) pp. 3170-3180. 6.